Combustion and Flame 168 (2016) 83–97

Contents lists available at ScienceDirect

Combustion and Flame

journal homepage: www.elsevier.com/locate/combustflame

Assessment of different chemistry reduction methods based on principal component analysis: Comparison of the MG-PCA and score-PCA approaches

Axel Coussement[a,*], Benjamin J. Isaac[a,d], Olivier Gicquel[b,c], Alessandro Parente[a]

[a] Université Libre de Bruxelles, Ecole Polytechnique de Bruxelles, Aero-Thermo-Mechanics Laboratory, Bruxelles, Belgium
[b] Ecole Centrale Paris, Grande Voie des Vignes, 92295 Chatenay-Malabry, France
[c] CNRS, UPR 288 Ç Laboratoire d'Energétique moléculaire et macroscopique, combustion, Grande Voie des Vignes, 92295 Chatenay-Malabry, France
[d] Department of Chemical Engineering, University of Utah, Salt Lake City, UT, 84112, USA

ARTICLE INFO

Article history:
Received 2 July 2015
Revised 22 March 2016
Accepted 22 March 2016
Available online 5 May 2016

Keywords:
Low-dimensional manifolds
Principal component analysis
Reacting flows
Reduced-order models

ABSTRACT

Two families of PCA based combustion model were recently developed: score-PCA and MG-PCA. This paper presents the first comparative study of the two aftermentioned methods. Both methods are first benchmarked on 1-D laminar flames of hydrogen–air and syngas–air, to verify the consistency of the approaches. The sensitivity to differential diffusion is carefully addressed and a rotation technique is proposed, to allow for using score-PCA with differential diffusion. Then, 2-D flame-turbulence interactions are considered, spanning a wide range of velocity and length scale ratios, to demonstrate the ability of PC-based combustion models to efficiently capture the behavior of different combustion regimes, from flamelet-like flames to distributed reaction regimes.

1. Introduction

The simulation of turbulent reacting systems using detailed (and reduced) kinetic mechanisms tends to be extremely expensive. For instance, the Direct Numerical Simulation of a reacting jet at high Reynolds number using detailed chemistry can already require millions of CPU hours, leading to unacceptable costs for more realistic configurations (see Chen et al. [1]). Therefore, there is a need for low order models such as low-dimensional manifold in the composition space that parameterize the full system with a reduced number of variables. In recent years, the potential for Principal Component Analysis (PCA) [2–4] towards the identification of these manifold has been investigated thoroughly, [5–12], with the main objective of defining a new family of reduced-order combustion models.

Starting from a thermo-chemical state space consisting of Q variables, PCA can provide a truncated set of q ($q < Q$) principal components, providing a low-dimensional representation of the manifold. Therefore, only q variables need to be taken into account instead of Q, accelerating the computation accordingly. Contrary to other reduction techniques, PCA models offer the advantage of not being bound to the original dataset used to train the model Coussement et al. [7].

Two families of PCA models were proposed. The first approach is based on the use of the transport equations for the scores (i.e the projection of the thermo-chemical state space on the PCA basis), and originates from the work of Sutherland and Parente [5,13]. It was further developed by Biglari and Sutherland [8] and Pope [14,15], using PCA in conjunction with non-linear regression techniques, to maximize the dimensionality reduction. Mirgolbabaei and Echekki [10,16] proposed the use of neural networks and investigated the potential of kernel PCA [7], to transform the initial problem into a non-linear feature space where the linear PCA is carried out. Finally Echekki and Mirgolbabaei [11] and Isaac et al. [12,17] provided the first *a posteriori* studies using the score-PCA approach.

Coussement et al. [9] proposed an alternative method based on PCA, the so-called Manifold Generated from PCA (MG-PCA). MG-PCA relies on classical transport equations for a reduced set of principal variables (PV), which are used to reconstruct the full thermo-chemical state using the information contained in the PC matrix. Isaac et al. [17] studied the behavior of MG-PCA on both 0-D auto-ignition and flame-vortex interactions, showing the capacity of MG-PCA based model trained on simple systems, to reproduce the behavior of more complex ones.

* Corresponding author. Fax:. +32 26502710.
E-mail address: axcousse@ulb.ac.be (A. Coussement).

http://dx.doi.org/10.1016/j.combustflame.2016.03.021
0010-2180/

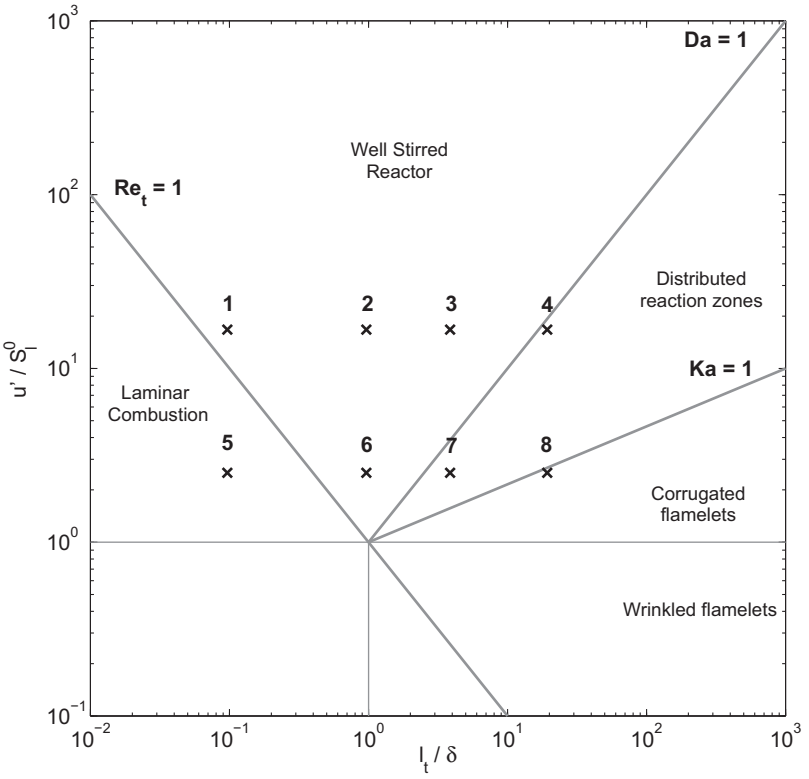

Fig. 1. Borghi diagram showing the different flame-turbulence interaction cases studied in this paper (×).

Despite recent research on PCA methods, only a few multidimensional cases were investigated, namely flame-turbulence and flame-vortex interaction cases with MG-PCA in DNS [17], and the Sandia flame F [11] with the score-PCA method in one dimensional turbulence (ODT) simulations. The aim of the present paper is to study the behavior of both score-PCA and MG-PCA models, for a wide range of combustion regimes in the framework of premixed turbulent combustion. First, 1-D laminar flames are used to generate the database for model training and verify the consistency of the method. Several equivalence ratios are considered, using syngas and hydrogen, paying particular attention to the effect of differential diffusion on the applicability of the methods. Various 2-D flame-turbulence interaction cases are then considered for both models and benchmarked against DNS, to investigated the ability of the methods to be applied outside of the original training manifold boundaries. The different cases investigated in the present study are shown in the Borghi diagram in Fig. 1

2. PCA method

The thermo-chemical state-space of a reacting system can be represented by the following variables: $[Y_1, \ldots, Y_{N_{sp}}, T, p]$, where Y_i is the mass fraction of species i, N_{sp} is the number of species, T is the temperature and p is the pressure. PCA is concerned with finding the best $q < Q$ dimensional representation of the original state-space. Then, it is sufficient to transport q variables to recover the missing $Q - q$ ones.

Considering a dataset $\mathbf{Y}(n \times Q)$, containing n samples of Q variables, the first operation to be considered is a centering and scaling of the dataset to give each variable the same importance during the analysis. Parente and Sutherland [6] and Isaac et al. [17] showed that the scaling of the dataset has great influence on the quality of PCA. This operation reads:

$$\widetilde{\mathbf{Y}} = (\mathbf{Y} - \overline{\mathbf{Y}})\mathbf{D}^{-1}, \tag{1}$$

where $\overline{\mathbf{Y}}$ is a $n \times Q$ matrix containing the mean of each variable and $\mathbf{D}$ is a $n \times Q$ matrix containing the standard deviation of each variable [6]. In the reminder of this paper, all the datasets are assumed to be centered and scaled for the sake of simplicity.

In order to perform PCA, the covariance matrix has to be evaluated,

$$\mathbf{S} = \frac{1}{n-1}\mathbf{Y}^t\,\mathbf{Y}. \tag{2}$$

$\mathbf{S}$ can be decomposed as:

$$\mathbf{S} = \mathbf{A}\,\mathbf{L}\,\mathbf{A}^t, \tag{3}$$

where $\mathbf{A}(Q \times Q)$ is the matrix of eigenvectors or Principal Components (PCs), associated to the eigenvalues of $\mathbf{S}$, $\mathbf{L}(Q \times Q)$, arranged in decreasing order of magnitude. Also, from Eqs. (2) and (3), it follows that $\mathbf{A}^{-1} = \mathbf{A}^t$. The matrix $\mathbf{A}$ defines a new basis composed of uncorrelated vectors.

The projection of the original sample onto the new basis defines the scores, called $\mathbf{Z}(n \times Q)$:

$$\mathbf{Z} = \mathbf{YA}. \tag{4}$$

Since the variance accounted by each PC eigenvector decreasing with its index it is possible to form a truncated basis retaining only the first q PCs. Thus, the original dataset can be approximated as:

$$\mathbf{Y} \approx \mathbf{Y}_q = \mathbf{Z}_q\mathbf{A}_q^t, \tag{5}$$

where $\mathbf{Z}_q(n \times q)$ and $\mathbf{A}_q(Q \times q)$ are computed from $\mathbf{Z}$ and $\mathbf{A}$ by retaining only the first q PCs (see [6] for details). Note that $\mathbf{A}_q^t$ is of size $(q \times Q)$ and is the transpose of $\mathbf{A}_q$. It is equivalent to the pseudo-inverse of $\mathbf{A}_q$, since the columns of $\mathbf{A}_q$ are made of orthonormal vectors.

3. Score-PCA approach

The score-PCA approach by Sutherland and Parente [5] is a direct application of PCA theory presented in the

previous section. If the original dataset includes n samples, PCA allows to compute an approximation of this dataset using Eq. (5).

The Q species transport equations are thus replaced by q scores equations, reducing the number of variables to be transported and therefore the CPU cost of the computation. The score transport equations reads [5]:

$$\frac{\partial \rho \mathbf{z}}{\partial t} + \nabla \cdot (\rho \mathbf{u} \otimes \mathbf{z}) = \nabla \cdot \rho D_{\mathbf{z}} \nabla \mathbf{z} + \Omega_{\mathbf{z}}, \tag{6}$$

where ρ is the density and $\mathbf{z} = \mathbf{Z}_i^t$ represent an individual score realization. Although the model in [5] applies to the full thermo-chemical state, for practical applications of score-PCA, it is recommended to limit the dataset $\mathbf{Y}$ to the chemical species [17]. In such a case, the diffusion matrix $D_{\mathbf{z}}$ and the reaction terms matrix Ω can easily be derived from the species matrix. The species conservation equations can be expressed as:

$$\frac{\partial \rho \mathbf{y}}{\partial t} + \nabla \cdot (\rho \mathbf{u} \otimes \mathbf{y}) = \nabla \cdot \rho D_{\mathbf{y}} \nabla \mathbf{y} + \Omega_{\mathbf{y}}, \tag{7}$$

with $\mathbf{y}$ is the chemical species vector. As for the scores, $\mathbf{y} = \mathbf{Y}_i^t$ is an individual realization of the chemical species (i.e. the species values at a particular point in space where Eq. (7) is applied). The dataset $\mathbf{Y}$ is obtained by sampling $\mathbf{y}$ at different locations in space. Using the score definition, one can write:

$$\mathbf{Z} = \mathbf{Y}\mathbf{A}_{\mathbf{q}}. \tag{8}$$

Using the definition in Eq. (8) in Eq. (7) and noticing that:

$$\nabla \mathbf{Y} = \nabla \mathbf{Z} \mathbf{A}_q^t, \tag{9}$$

it is fairly easy to derive an expression for the score diffusion coefficient,

$$\mathbf{D}_{\mathbf{z}} = \mathbf{A}_q^t D_{\mathbf{y}} \mathbf{A}_q \tag{10}$$

and for the score source term,

$$\Omega_{\mathbf{z}} = \Omega_{\mathbf{y}} \mathbf{A}_q, \tag{11}$$

where $D_{\mathbf{y}}$ is the diffusion matrix of species $\mathbf{y}$ and $\Omega_{\mathbf{y}}$ are the corresponding source terms per unit mass.

Eq. (6) is easy to compute in a reactive flow solver but still requires closure at the boundaries. This closure is achieved using:

$$\mathbf{z}|_{boundary} = \mathbf{y}|_{boundary} \mathbf{A}_q, \tag{12}$$

where $\mathbf{y}|_{boundary}$ are the species mass fraction values to be enforced at the boundaries. In the case of the Navier–Stokes equations, the viscous fluxes to be enforced on the boundary can be derived easily from [18,19].

4. MG-PCA approach

The MG-PCA approach also relies on PCA but is based on the resolution of classic transport equations for a selected number of transported species, while the non-transported ones are reconstructed using PCA, considering Eq. (5):

$$\mathbf{Z} \approx \mathbf{Y}_q \mathbf{A}_q. \tag{13}$$

However, $\mathbf{Z}$ can also be found by using a subset of species $\mathbf{Y(q)}$ and a subset of the $\mathbf{A}_q$ matrix, $\mathbf{A(q)}_q$:

$$\mathbf{Z} = \mathbf{Y}(\mathbf{q})\mathbf{A}(\mathbf{q})_q. \tag{14}$$

Introducing Eq. (14) in Eq. (5) we get:

$$\mathbf{Y} \approx \mathbf{Y}_q = \mathbf{Y}(\mathbf{q})\mathbf{B}_q, \tag{15}$$

where $\mathbf{B}_q$ is a $(q \times Q)$ matrix derived from $\mathbf{A}_q$ [17], allowing the reconstruction of $(Q - q)$ non-transported species from the q transported ones.

Similarly to score-PCA, MG-PCA allows reducing the number of transport equation to $q < Q$. Additional analysis is, however, required to determine the variables to transport. Several methods exist to this purpose and a full sensitivity to them is shown in [17]. Here the B2 backward selection method is used. The choice of the variables is also very important from the numerical perspective, to ensure stability of the solution.

5. Test cases and reduced-order model generation

The following section briefly discusses the test cases selected for the assessment of the models. First the database used to generate PCA has to be chosen. Here, the database consists of a converged one-dimensional freely propagating laminar flame. To avoid any bias, the same explicit solver is used to generate the database and to test the models. Convergence is reached when the relative change in the manifold is below 10^{-6} for species and temperature.

Eight different databases are used corresponding to two different fuels: syngas and hydrogen each at two different equivalence ratios with and without differential diffusion. In each instance both PCA-based methods will be compared, they will be trained with the same database.

For the hydrogen cases, the following equivalence ratios are considered: $\phi = 0.75$ and $\phi = 1$, with and without differential diffusion. For each case, the grid is composed of 5121 points with a spacing of $6.25\,10^{-6}$ m. Pressure is set to 101, 325 Pa and inlet temperature is 300 K. Inlet velocity is different for each equivalence ratio: $u = 1.25$m/s at $\phi = 0.75$ and $u = 1.5$ m/s at $\phi = 1$. The chemical scheme is the one from Ó˜Conaire et al. [20], containing 9 species: Y_H, Y_{H_2}, Y_O, Y_{O_2}, Y_{OH}, Y_{H_2O}, Y_{N_2}, Y_{HO_2} and $Y_{H_2O_2}$.

For the syngas (50% H_2/50% CO by vol.) cases, two different equivalence ratios are considered: $\phi = 0.7$ and $\phi = 1$, with and without differential diffusion. The grid, pressure and inlet temperature are exactly the same as for the hydrogen cases. Inlet velocities are set to $u = 0.5$ m/s at $\phi = 0.7$, and $u = 0.65$ m/s at $\phi = 1$. The chemical scheme is taken from Davis et al. [21], containing 12 species: Y_{N_2}, Y_{O_2}, Y_{H_2}, Y_{H_2O}, $Y_{H_2O_2}$, Y_{CO}, Y_{CO_2}, Y_O, Y_H, Y_{OH}, Y_{HO_2} and Y_{HCO}.

To generate the reduced models, PCA is carried out on one of the eight database, depending on the computation to be performed. The number of variables (either scores or species) to be transported is chosen to allow a for quasi-exact reconstruction of the original dataset. If not, the method could introduce large errors in the calculation of thermodynamic data and source terms, leading to numerical instabilities. The reconstruction is assumed to be quasi-exact when a coefficient of determination, R^2, greater than 0.999 is obtained for all variables (see [9]). By doing so on each database, one can see that 7 PCs must be retained for all the syngas cases and 6 for the hydrogen cases.

For MG-PCA, one must still choose the species to be transported. The species are selected using the B2 criterion [17]:

- Y_H, Y_O, Y_{OH}, Y_{HO_2}, Y_{H_2O} and $Y_{H_2O_2}$ for the hydrogen cases.
- Y_{H_2O}, $Y_{H_2O_2}$, Y_O, Y_H, Y_{OH}, Y_{HO_2} and Y_{HCO} for the syngas cases.

It is worth noting that the number of variables and the species transported depends only on the fuel. This yields a database which contains a 9×6 matrix and two 9×1 vectors (centering and scaling) for the hydrogen scheme, and a 12×7 matrix and two 12×1 vectors for syngas. It is also interesting to note that, using different equivalence ratios or different diffusion law assumptions, the number of components or variables to be transported does not change.

From a manifold reduction point of view, using 6 PCs with hydrogen test case do not lead to a reduction in the degrees of freedom of the problem when $Le = 1$. However when the differential diffusion is taken into account, a reduction of 1 degree of freedom

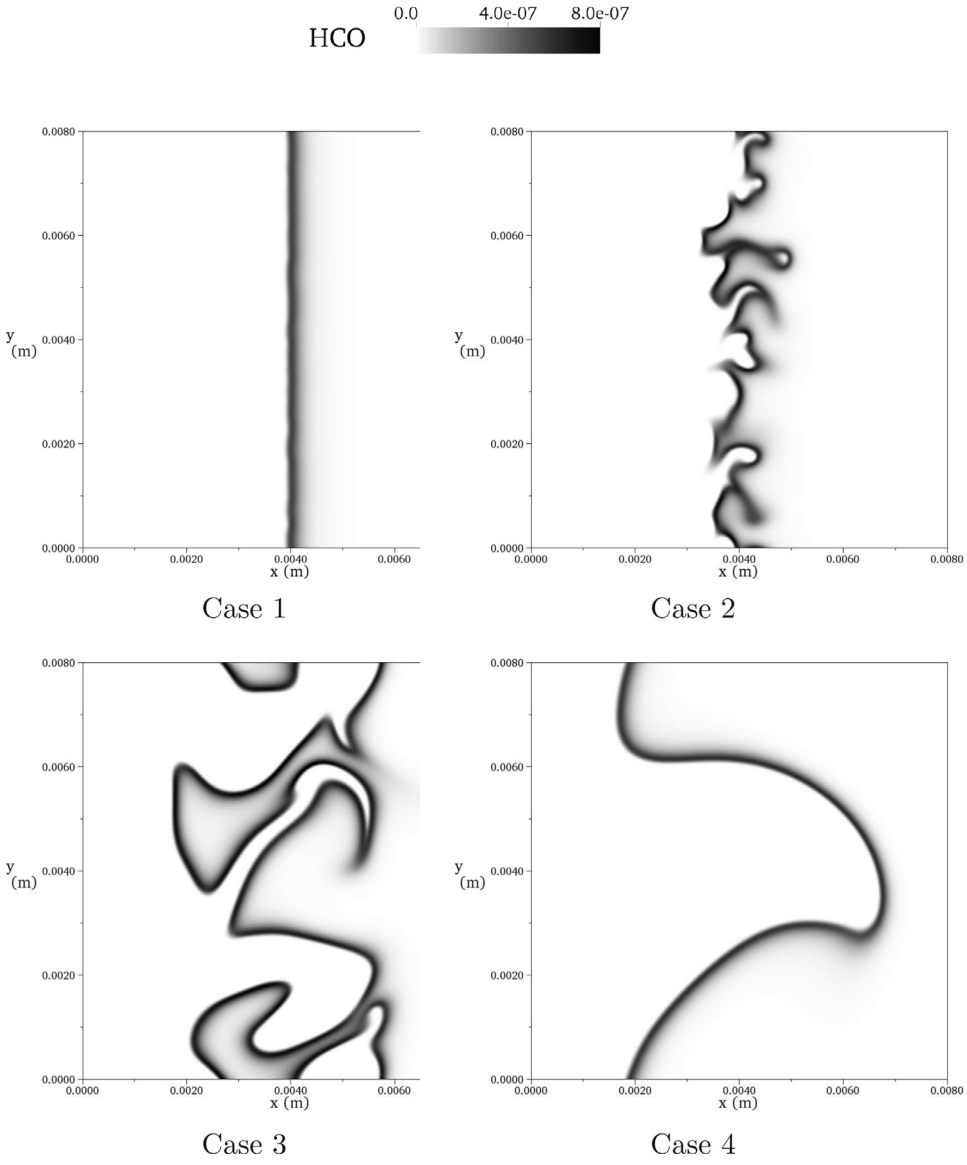

Fig. 2. HCO field for cases 1 to 4.

is achieved (15 %). In the syngas case, using 7 PCs leads to a reduction of 1 degree of freedom out of 8 (12.5 %) for $Le = 1$, and 4 degrees of freedom when $Le \neq 1$, providing a reduction of 50 %. The reduction obtained in this paper is in line with previous investigations [7,9–12]

Although coupling PCA with non-linear regression [11,12] has the potential of ensuring very strong compression, the approach strongly relies on the ability of the chosen non-linear model to reproduce the system physics. On the other hand, keeping the full original mechanism results in lower reduction but allows, at the same time, to increase the range of applicability and the generality of the reduced models. The present paper aims to focus on the latter aspect, to allow a throughout comparison of the two methods.

Once both reduced methods are trained on the laminar flame simulations, they are benchmarked against each other and with respect to DNS. First the eight one-dimensional freely propagating laminar flames used to train the model are considered. The relative simplicity of these cases is ideal to benchmark the different models. In all cases, the database used to perform PCA is the flame itself, therefore both methods are *a priori* expected to yield perfect results.

Then, eight-flame turbulence interactions cases are considered covering various regimes (see Fig. 1). The objective is to investigate the range of applicability of the reduced models, trained with the same single freely propagating laminar premixed flame, when changing the Reynolds and Damkohler numbers. The wide range of regimes spanned by our investigation can be appreciated in Fig. 2, which shows Y_{HCO} distribution for four of the eight cases, namely cases 1 to 4. Not only flamelet-like regimes are considered, but also distributed reaction zones, which show significant deviations with respect to the original training dataset.

All simulations are performed using the compressible solver YWC developed at the EM2C Laboratory, using a CHEMKIN-like [22] formalism for the computation of thermo-chemical properties (see [18,19] for details).

5.1. 1-D flame cases

The present section discusses the results obtained using the score-PCA and MG-PCA methods on the 1-D flames. In order to compare them, each 1-D flame was simulated from the DNS solution until convergence was once again reached. The criterion

Table 1
Maximum errors, $\epsilon_{k,\text{model}}$, of MG-PCA and score-PCA approaches for the hydrogen test cases with $Le = 1$.

Species	$\epsilon_{k,\text{MG-PCA}}$ (%)	$\epsilon_{k,\text{S-PCA}}$ (%)	$\epsilon_{k,\text{MG-PCA}}$ (%)	$\epsilon_{k,\text{S-PCA}}$ (%)
	$\phi = 0.75$	$\phi = 0.75$	$\phi = 1$	$\phi = 1$
Y_{N_2}	≈ 0	≈ 0	≈ 0	≈ 0
Y_H	0.0036	0.3262	0.0495	2.5381
Y_{H_2}	0.0018	0.1783	0.0259	1.3237
Y_O	0.0031	0.3483	0.0464	2.3372
Y_{O_2}	0.0013	0.1331	0.0237	1.2063
Y_{OH}	0.0023	0.3056	0.0321	1.5732
Y_{H_2O}	0.0016	0.1569	0.0230	1.1783
Y_{HO_2}	0.0052	0.2461	0.0815	4.4077
$Y_{H_2O_2}$	0.0043	0.2726	0.0671	3.6362

Table 2
Maximum errors, $\epsilon_{k,\text{model}}$, of MG-PCA and score-PCA approaches for the hydrogen test cases with $Le \neq 1$.

Species	$\epsilon_{k,\text{MG-PCA}}$ (%)	$\epsilon_{k,\text{S-PCA}}$ (%)	$\epsilon_{k,\text{S-PCA}}$ (%) VARIMAX	$\epsilon_{k,\text{MG-PCA}}$ (%)	$\epsilon_{k,\text{S-PCA}}$ (%)	$\epsilon_{k,\text{S-PCA}}$ (%) VARIMAX
	$\phi = 0.75$	$\phi = 0.75$	$\phi = 0.75$	$\phi = 1$	$\phi = 1$	$\phi = 1$
Y_{N_2}	≈ 0	≈ 0	≈ 0	≈ 0	≈ 0	≈ 0
Y_H	3.9219	1.7359	2.1356	1.5592	0.6226	1.2135
Y_{H_2}	8.1131	3.2091	6.1245	2.6318	1.2782	1.8902
Y_O	2.3025	0.7016	1.2432	2.0334	1.2435	2.1356
Y_{O_2}	1.8564	3.0198	2.1466	0.2751	1.1857	0.6721
Y_{OH}	2.7657	1.0816	5.1245	1.0733	0.7062	3.1245
Y_{H_2O}	2.2144	3.2597	5.1246	0.4388	1.1190	1.3456
Y_{HO_2}	17.5078	7.0385	6.2211	3.8679	4.9692	4.5311
$Y_{H_2O_2}$	11.6380	5.3595	7.1241	2.0933	1.1518	3.1345

Table 3
Maximum errors, $\epsilon_{k,\text{model}}$, of MG-PCA and score-PCA approaches for the syngas test cases with $Le = 1$.

Species	$\epsilon_{k,\text{MG-PCA}}$ (%)	$\epsilon_{k,\text{S-PCA}}$ (%)	$\epsilon_{k,\text{MG-PCA}}$ (%)	$\epsilon_{k,\text{S-PCA}}$ (%)
$\phi = 0.7$	$\phi = 0.7$	$\phi = 1$	$\phi = 1$	
Y_{N_2} ≈ 0	≈ 0	≈ 0	≈ 0	
Y_{O_2}	0.2679	0.3651	$5.7009\ 10^{-4}$	0.6804
Y_{H_2}	0.6005	0.2771	$8.5543\ 10^{-4}$	1.0311
Y_{H_2O}	0.7011	0.7757	$7.8693\ 10^{-4}$	0.9444
$Y_{H_2O_2}$	1.1133	0.3086	0.0021	2.5878
Y_{CO}	0.2092	0.2093	$3.3805\ 10^{-4}$	0.4034
Y_{CO_2}	0.1994	0.2361	$3.9419\ 10^{-4}$	0.4677
Y_O	1.3036	0.9571	0.0015	1.7437
Y_H	2.7675	2.1277	0.0016	1.8974
Y_{OH}	2.8536	1.5922	$7.9389\ 10^{-4}$	0.9402
Y_{HO_2}	1.2945	0.4642	0.0026	3.1401
Y_{HCO}	1.7357	0.6363	0.0032	3.9520

retained for assessing the quality of the models is the maximum error relative to the maximum value for each species $\epsilon_{k,\text{model}}$:

$$\epsilon_{k,\text{model}} = \max \frac{|Y_{k,\text{model}} - Y_{k,\text{DNS}}|}{\max Y_{k,\text{DNS}}}, \tag{16}$$

where $Y_{k,\text{model}}$ is the mass fraction of species k, computed with the reduced model, and $Y_{k,\text{DNS}}$ the mass fraction of species k, computed with DNS. As only the maximum is taken into account, the criterion is very severe. To have a sound comparison between MG-PCA and score-PCA, results were post-processed so that the point corresponding to $T = 1000\,\text{K}$ is at the same location with respect to the DNS solution. The results are presented in Tables 1–4.

The error in the laminar flame speed predictions, S_l, is presented in Tables 5 and 6 for hydrogen and syngas, respectively. The deviation is estimated by computing the relative error on the laminar flame speed value as provided by the PCA models with respect to the DNS solution. The S_l value is computed as:

$$S_l = -\frac{1}{\rho Y_F} \int_{mesh} \dot{\omega}_F \, dx, \tag{17}$$

Table 4
Maximum errors, $\epsilon_{k,\text{model}}$, of MG-PCA and score-PCA approaches for the syngas test cases with $Le \neq 1$.

Species	$\epsilon_{k,\text{MG-PCA}}$ (%)	$\epsilon_{k,\text{S-PCA}}$ (%)	$\epsilon_{k,\text{S-PCA}}$ (%) VARIMAX	$\epsilon_{k,\text{MG-PCA}}$ (%)	$\epsilon_{k,\text{S-PCA}}$ (%)	$\epsilon_{k,\text{S-PCA}}$ (%) VARIMAX
	$\phi = 0.7$	$\phi = 0.7$	$\phi = 0.7$	$\phi = 1$	$\phi = 1$	$\phi = 1$
Y_{N_2}	≈ 0	≈ 0	≈ 0	≈ 0	N/A	≈ 0
Y_{O_2}	1.1515	1.3284	1.2134	0.4905	N/A	2.6531
Y_{H_2}	10.4504	1.0814	3.2464	6.7174	N/A	2.8506
Y_{H_2O}	1.0337	4.0001	1.3461	0.7402	N/A	4.2862
$Y_{H_2O_2}$	4.8962	6.1756	5.6799	3.3443	N/A	10.6046
Y_{CO}	1.0899	2.0329	0.9235	0.4527	N/A	0.9798
Y_{CO_2}	2.6966	2.1660	2.3461	0.5863	N/A	1.1895
Y_O	4.3250	2.9284	3.1344	2.4246	N/A	3.9111
Y_H	2.1114	2.7048	4.1211	1.1407	N/A	2.9958
Y_{OH}	3.6944	3.3695	4.1241	1.1500	N/A	2.6153
Y_{HO_2}	5.9161	7.1765	10.1351	4.5448	N/A	19.2864
Y_{HCO}	4.9373	6.7068	7.8912	3.0235	N/A	9.0309

Table 5
Relative error on the laminar flame speed for hydrogen test cases.

Condition	S_l error in % MG-PCA	S_l error in % Score-PCA	S_l error in % Score-PCA and VARIMAX
$\phi = 0.75$ $Le = 1$	$< 10^{-4}$	$< 10^{-4}$	–
$\phi = 1$ $Le = 1$	$< 10^{-4}$	$< 10^{-4}$	–
$\phi = 0.75$ $Le \neq 1$	1.2183	7.823	0.3139
$\phi = 1$ $Le \neq 1$	1.5597	8.125	0.667

Table 6
Relative error on the laminar flame speed for syngas test cases.

Condition	S_l error in % MG-PCA	S_l error in % Score-PCA	S_l error in % Score-PCA and VARIMAX
$\phi = 0.75$ $Le = 1$	$< 10^{-4}$	$< 10^{-4}$	–
$\phi = 1$ $Le = 1$	$< 10^{-4}$	$< 10^{-4}$	–
$\phi = 0.75$ $Le \neq 1$	0.620	12.039	0.145
$\phi = 1$ $Le \neq 1$	0.401	–	0.243

where the subscript F indicates the fuel and $\dot{\omega}_F$ its reaction rate. The syngas case with $Le \neq 1$ and $\phi = 1$ was unstable when computed using the score-PCA approach, so that data is not available for this case. This is linked to the reconstruction of the diffusive fluxes as explained below.

In terms of maximum errors (ϵ_k), when $Le = 1$, results are in favor of MG-PCA, where errors tends to be one order of magnitude smaller than for score-PCA. However, even for the latter, errors are still very low (1–2 %). Both models are able to accurately reproduce the flame structure, indicating that the reconstruction error on the species are small enough to avoid biasing the source terms and transport properties.

When considering the $Le \neq 1$ cases, Table 2 and 4 show that both methods are comparable. However when looking at the laminar flame speed error, it is clear that the MG-PCA approach is able to capture the correct flame speed, while score-PCA displays large errors. To emphasize this, Fig. 3 shows a comparison of the two methods for the syngas case at $\phi = 0.7$. We can observe the score-PCA approach cannot deal with cases where differential diffusion is taken into account.

The overestimation of S_l by the score-PCA can be due to an error in the evaluation of the diffusion fluxes and/or source terms. As indicated above, the latter can be attributed to the non linear propagation of the error on the reconstructed species, whereas the former is due to the appearance of negative off-diagonal source terms in the diffusion matrix. As the errors are observed only on the predictions of S_l with differential diffusion, the origin of the errors lies in the diffusion modeling. Indeed, the score diffusion matrix (Table 7) for hydrogen at $\phi = 0.75$ and

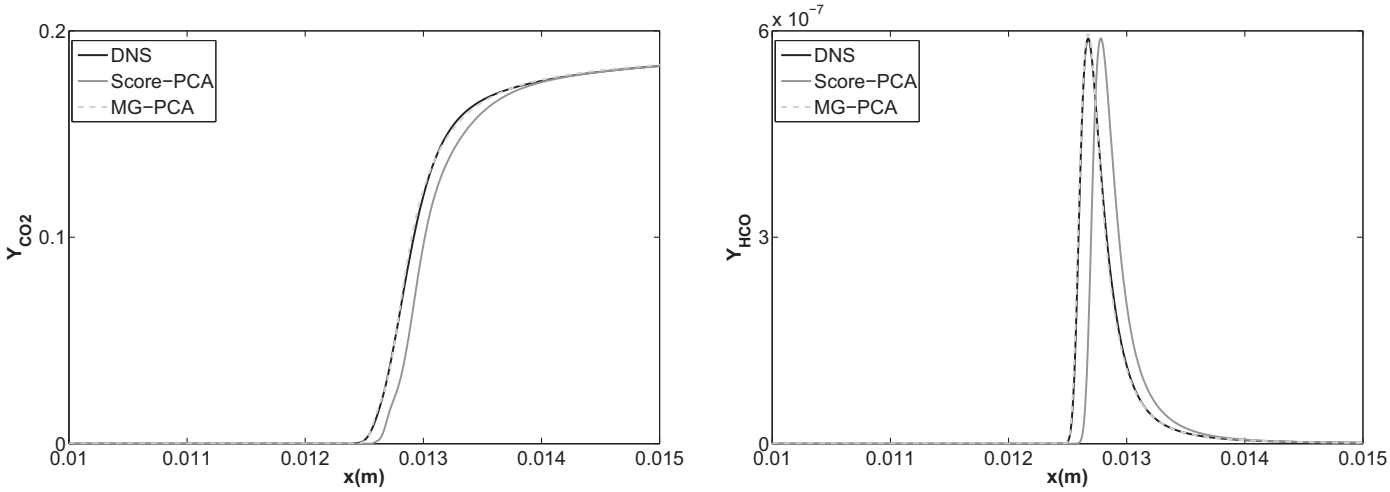

Fig. 3. Comparison of Y_{CO_2} and Y_{HCO} predictions by MG-PCA and score-PCA, for the syngas test case.

Table 7
Score diffusion matrix for the hydrogen case at $\phi = 0.75$ and $Le \neq 1$.

	z_1	z_2	z_3	z_4	z_5	z_6
z_1	1.2303 10^{-3}	1.6157 10^{-4}	−2.8651 10^{-4}	−4.7042 10^{-4}	−4.0757 10^{-5}	2.9592 10^{-4}
z_2	1.6157 10^{-4}	1.2096 10^{-3}	−7.5123 10^{-4}	−6.1785 10^{-4}	−7.7428 10^{-5}	4.8711 10^{-4}
z_3	−2.8651 10^{-4}	−7.5123 10^{-4}	1.5325 10^{-3}	7.4382 10^{-4}	9.4947 10^{-5}	−5.9447 10^{-4}
z_4	−4.7042 10^{-4}	−6.1785 10^{-4}	7.4382 10^{-4}	1.8451 10^{-3}	5.1270 10^{-5}	−7.1834 10^{-4}
z_5	−4.0757 10^{-5}	−7.7428 10^{-5}	9.4947 10^{-5}	5.1270 10^{-5}	6.6198 10^{-4}	−1.8693 10^{-4}
z_6	2.9592 10^{-4}	4.8711 10^{-4}	−5.9447 10^{-4}	−7.1834 10^{-4}	−1.8693 10^{-4}	1.3889 10^{-3}

Table 8
Score diffusion matrix for the hydrogen case at $\phi = 0.75$ and $Le \neq 1$ using VARIMAX rotation.

	z_1	z_2	z_3	z_4	z_5	z_6
z_1	1.1778 10^{-3}	−5.0800 10^{-6}	−3.8897 10^{-5}	2.1682 10^{-5}	−2.1537 10^{-5}	4.4452 10^{-5}
z_2	−5.0800 10^{-6}	5.9260 10^{-4}	−2.3508 10^{-7}	−2.2615 10^{-7}	2.4600 10^{-7}	−4.0640 10^{-7}
z_3	−3.8897 10^{-5}	−2.3508 10^{-7}	3.6705 10^{-3}	9.9370 10^{-7}	−9.2803 10^{-7}	2.7471 10^{-6}
z_4	2.1682 10^{-5}	−2.2615 10^{-7}	9.9370 10^{-7}	9.0556 10^{-4}	−9.7649 10^{-7}	1.6148 10^{-6}
z_5	−2.1537 10^{-5}	2.4600 10^{-7}	−9.2803 10^{-7}	−9.7649 10^{-7}	5.9742 10^{-4}	−1.7610 10^{-6}
z_6	4.4452 10^{-5}	−4.0640 10^{-7}	2.7471 10^{-6}	1.6148 10^{-6}	−1.7610 10^{-6}	9.2465 10^{-4}

$Le \neq 1$, shows negative cross-diffusion terms. The diagonal terms do not appear to be dominant. Some negative off-diagonal terms are also reported in other PCA studies [10,16]. When differential diffusion is not taken into account, the off-diagonal terms vanish. Indeed, as the diffusion coefficients, D_i, are equal for all the species, $D_i = D$, Eq. (10) becomes:

$$D_{\mathbf{z}} = D\,\mathbf{A}_q^t\,\mathbf{A}_q. \tag{18}$$

Considering that, by definition, $\mathbf{A}_q^t\,\mathbf{A}_q = \mathbf{I}$, we obtain $D_{\mathbf{z}} = D\,\mathbf{I}$, which implies that no off-diagonal terms are present.

Handling differential diffusion with the score approach requires the transformation of the diffusion matrix, to make it diagonally dominant and allow the use of Fick's law. This can be accomplished using the PC rotation. Through rotation, the weights can be redefined to meet an alternative criteria. In particular, rotation is aimed at attaining a simple structure for $\mathbf{A}_q$, so that weights on a PC are either close to unity or close to zero and, thus, variables have large weights on only few or (ideally) one PC. The most common orthogonal rotation is based on the maximization of the VARIMAX criterion Kaiser [23]. Verbally, such rotation concentrates the amount of variance explained for any of the original variables on single PCs. After VARIMAX rotation, $\mathbf{A}_q$ will generally have fewer large coefficients in its columns. Using VARIMAX implies that the error associated to the reduction is also the same after the rotation. The diffusion matrix presented in Table 8 displays more dominant diagonal terms. Also this method conserves the global variance accounted for by the scores [23].

Table 9
Parameters used for the eight flame-turbulence interaction cases: l_e and u_{up} are the Passot–Pouquet Parameters [24], u_{conv} is the convection speed superimposed on the turbulence spectrum, Re_t and l_t are respectively the turbulent Reynolds number and integral length scale.

	l_e(m)	u_{up}(m/s)	u_{conv}(m/s)	Re_t	l_t
Case 1	5 10^{-5}	10	10	14.231	1.899 10^{-5}
Case 2	5 10^{-4}	10	10	1423	1.899 10^{-3}
Case 3	2 10^{-3}	10	10	22,781	3.038 10^{-2}
Case 4	1 10^{-2}	10	10	569,544	7.596 10^{-1}
Case 5	5 10^{-5}	2	1	0.565	3.798 10^{-6}
Case 6	5 10^{-4}	2	1	56.952	3.798 10^{-4}
Case 7	2 10^{-3}	2	1	911	6.077 10^{-3}
Case 8	1 10^{-2}	2	1	22,781	1.519 10^{-1}

In their work, Echekki and Mirgolbabaei [11] also proposed a rotation of the diffusion matrix to attenuate the issue of the off-diagonal terms, using a minimization algorithm. While interesting, such an approach does not *a priori* guarantee that the global variance accounted for by the score will be kept, while this is ensured by VARIMAX rotation.

All cases with $Le \neq 1$ were recomputed using these rotated PCs. Results for ϵ_k are given in Tables 2 and 4, while Tables 5 and 6 report the laminar flame speed errors. Moreover, the syngas

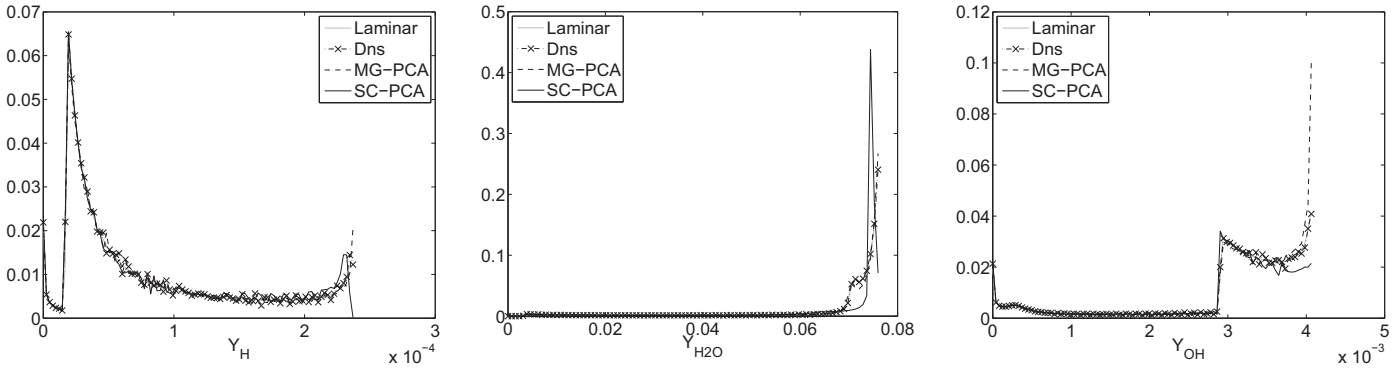

Fig. 4. Conditional PDF of Y_H, Y_{H_2O} and Y_{OH} for case 1.

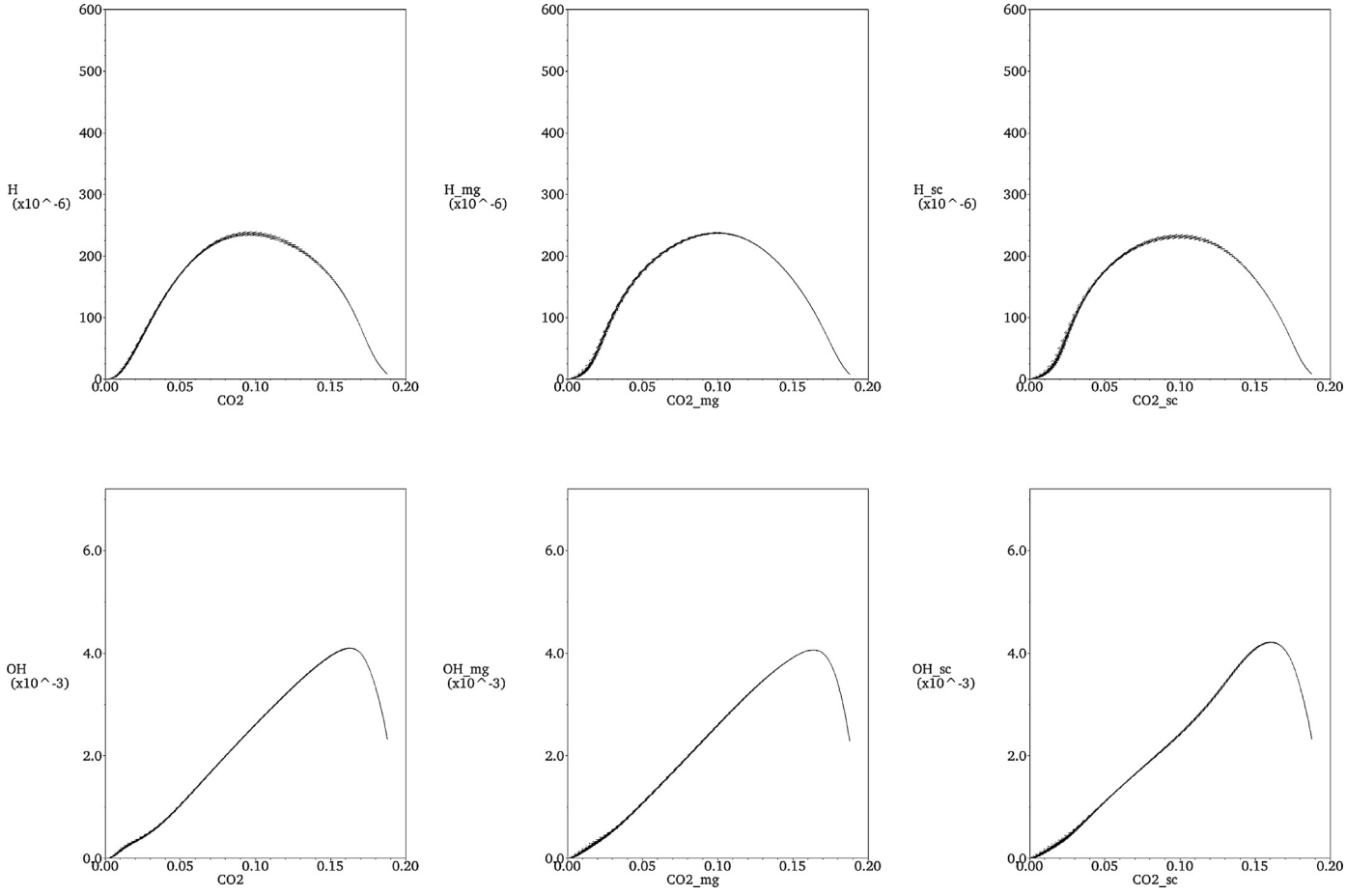

Fig. 5. Scatter plots of Y_H vs Y_{CO_2} for case 1, using DNS (left), MG-PCA (center) and score-PCA (right).

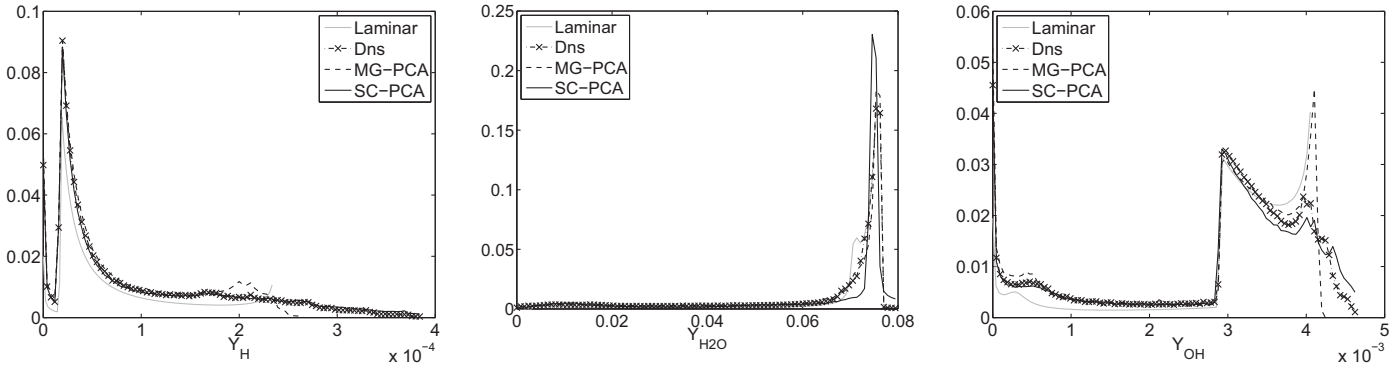

Fig. 6. Conditional PDF of Y_H, Y_{H_2O} and Y_{OH} for case 2.

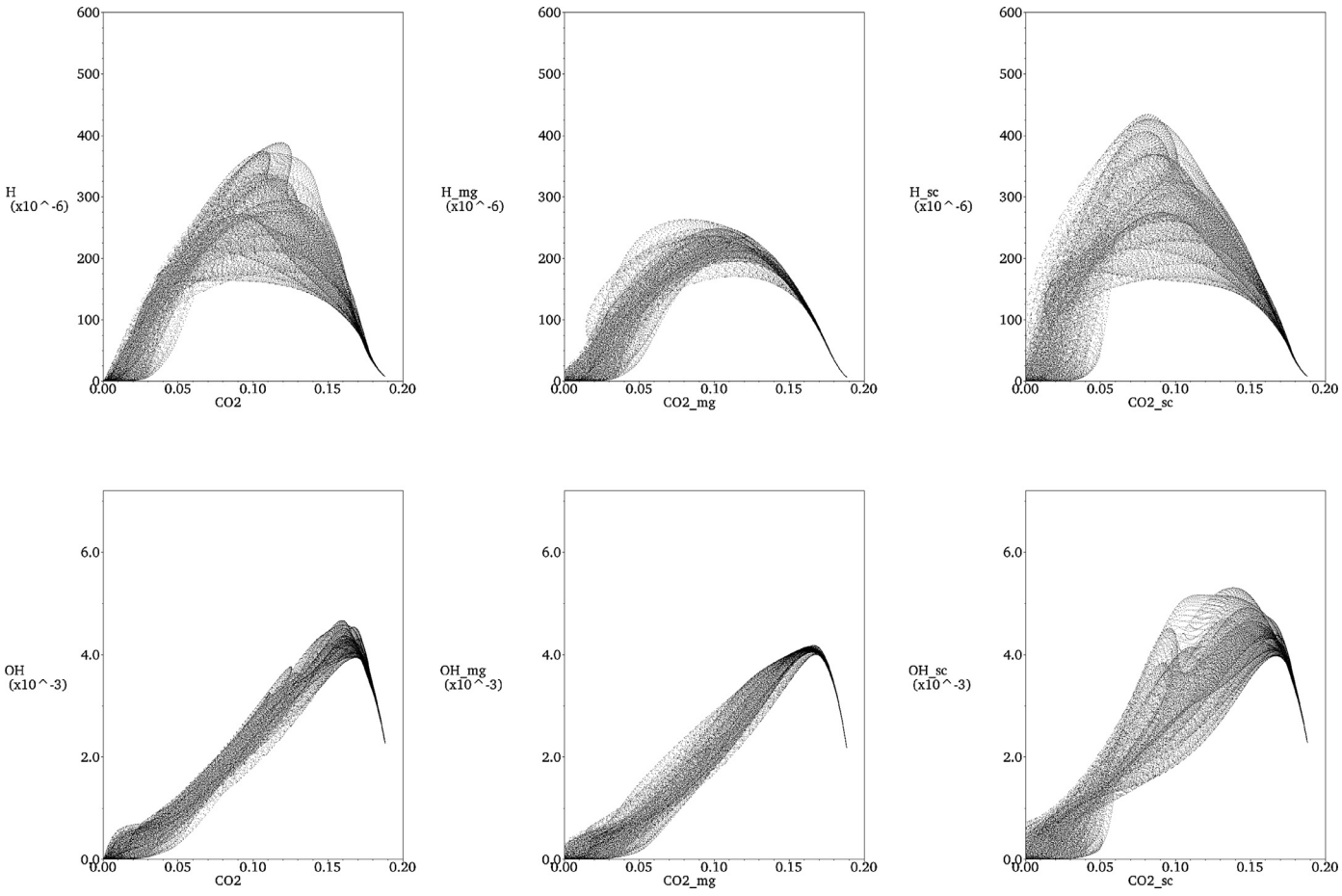

Fig. 7. Scatter plots of Y_H vs Y_{CO_2} for case 2, using DNS (left), MG-PCA (center) and score-PCA (right).

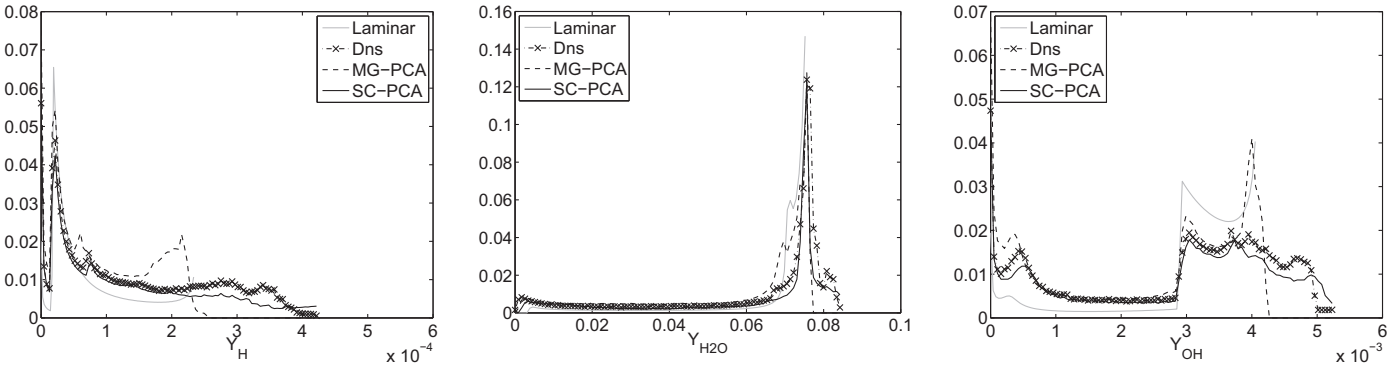

Fig. 8. Conditional PDF of Y_H, Y_{H_2O} and Y_{OH} for case 3.

case at $\phi = 1$ using rotation is now stable. After rotation, score-PCA outperforms MG-PCA both in terms of species mass fraction distribution and laminar flame speed predictions. Such result can be directly linked to the condition number of matrices $\mathbf{A}_q$ and $\mathbf{B}_q$, used for score-PCA and MG-PCA, respectively. In the case of score-PCA, $\mathbf{A}_q$ is composed of orthogonal vectors by construction and, since the species are centered and scaled (i.e. normalized), it results in a perfectly conditioned matrix (condition number equal to one). On the other hand, $\mathbf{B}_q$ used in MG-PCA displays a condition number ranging from 1.54 to 3.53, depending on the cases. This is explained by the partial correlation left in the transported species, even when selecting the most uncorrelated ones of the sample [9]. Adding to this the fact that the transported species can span different order of magnitudes (while the scores are scaled), the numerical reconstruction error will be eventually higher for MG-PCA.

Finally it should be stressed that off-diagonal terms, while negligible, are still present in the diffusion matrix. They could generate numxerical instabilities, due to error amplification, for very long simulations. However, we did not find any evidence of this in the present study.

5.2. Flame turbulence interaction

The present Section aims to assess the behavior of the score-PCA (using rotation) and MG-PCA models when outside the bounds defined by the training dataset. As showed in Coussement et al. [9], PCA methods are able to predict the state-space of a stretched

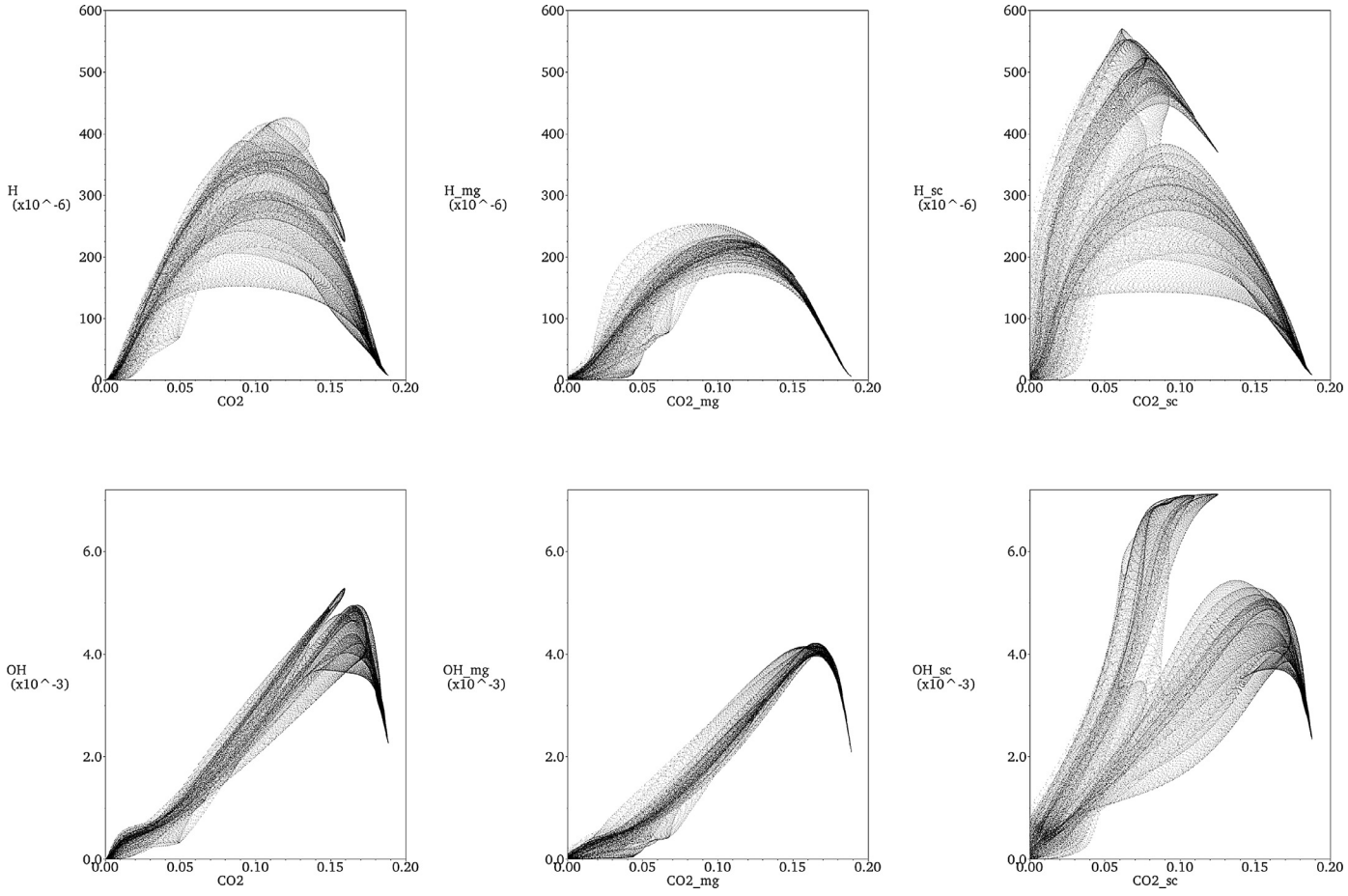

Fig. 9. Scatter plots of Y_H vs Y_{CO_2} for case 3, using DNS (left), MG-PCA (center) and score-PCA (right).

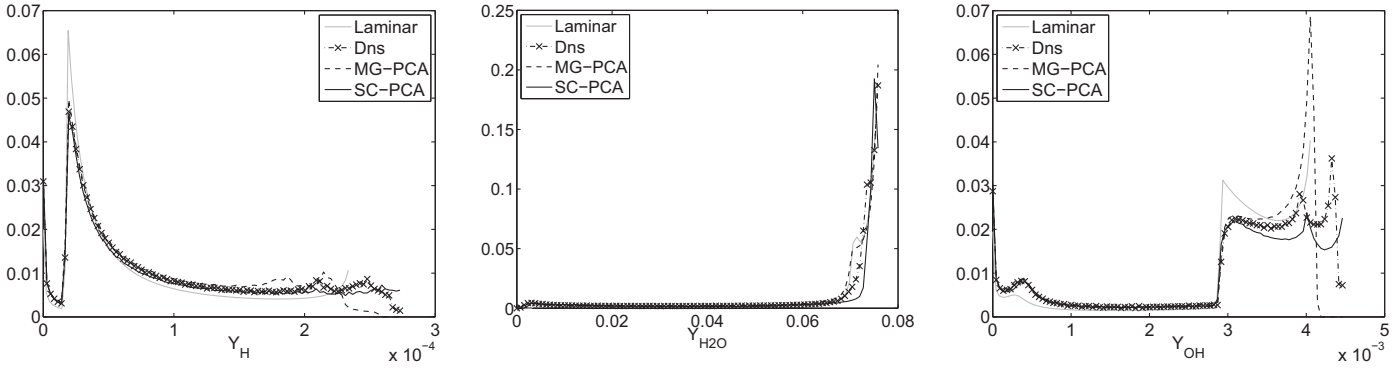

Fig. 10. Conditional PDF of Y_H, Y_{H_2O} and Y_{OH} for case 4.

flame, using a model built with an undisturbed laminar flame. To further this enquiry, eight flame-turbulence interaction cases are simulated using four different eddy sizes and two maximum eddy velocities, to cover several combustion regimes (see Fig. 1). Each case is computed 3 times, using DNS, MG-PCA and score-PCA with VARIMAX rotation.

The baseline for all cases is the syngas laminar flame at $\phi = 0.7$ which is extended on the y-axis on a 2-D domain of 640 $\times$ 640 points, with a mesh spacing of $1.25\,10^{-6}$m. At $x = x_{\min}$ the boundary condition fixes a constant speed with a superimposed turbulent field at a temperature of 300 K. At $x = x_{\max}$, an outlet boundary is imposed with $p = 101,325$ Pa. Remaining boundary conditions ensure periodicity along the y-axis. The turbulent field is obtained using the Passot–Pouquet spectrum [24]. The numerical parameters for the different cases are summarized in Table 9. Figure 2 shows the Y_{HCO} field for cases 5 to 8, emphasizing the wide spectrum of conditions considered here. All numerical simulations are performed using differential diffusion, they are run for 0.5 ms, ensuring that manifold statistics do not evolve anymore with time.

In order to assess the quality of the results, Coussement et al. [9] and Isaac et al. [17] used a simple comparison of species scatter plots. While this provides valuable general information of the performance of the method, this type of comparison cannot provide a quantitative assessment of the agreement between reduced models and DNS.

In this study, the probability density function (PDF) of the species mass fraction are used to benchmark the reduced-order

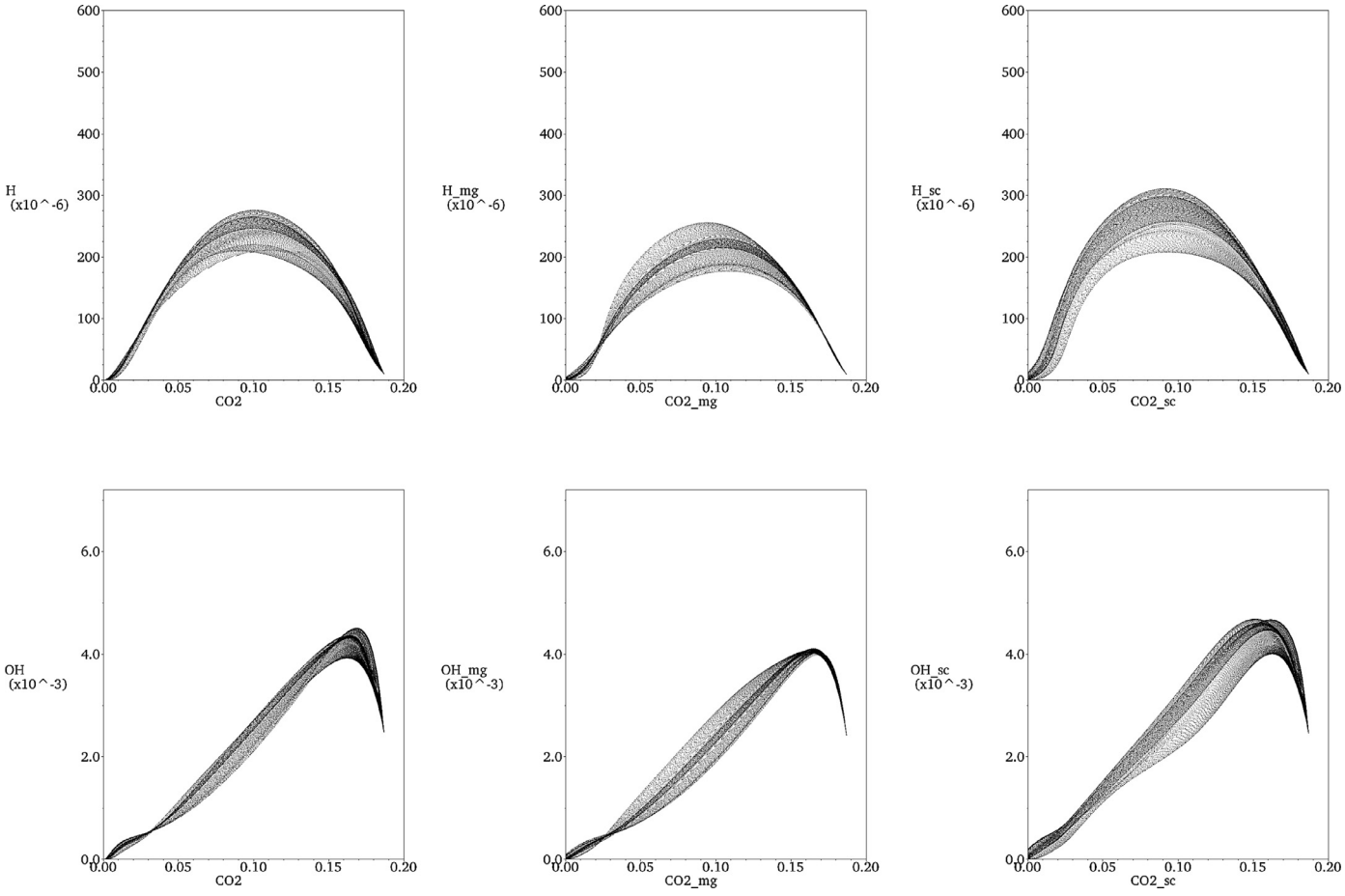

Fig. 11. Scatter plots of Y_H vs Y_{CO_2} for case 4, using DNS (left), MG-PCA (center) and score-PCA (right).

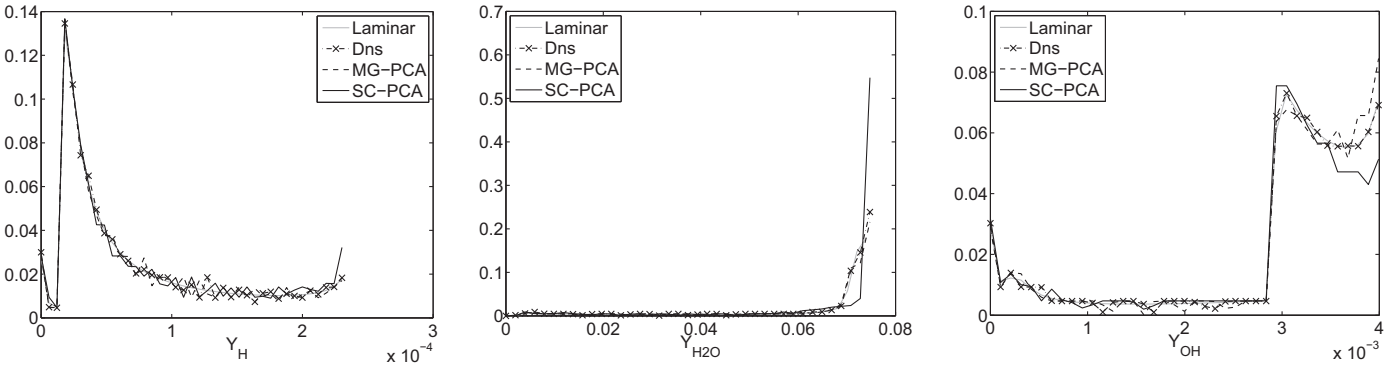

Fig. 12. Conditional PDF of Y_H, Y_{H_2O} and Y_{OH} for case 5.

model performances to DNS. Indeed, if the models behaved perfectly, their PDFs should overlap with those provided by DNS. Thus, difference between model and DNS PDFs will indicate sources of error from the reduced models. In order to discard fresh and burned gases (over-represented in the computational domain [7]), only the nodes where $Y_{HCO} > 10^{-8}$ are used to compute the PDFs. The PDFs of Y_H, Y_{H_2O} and Y_{OH} are considered, along with the PDF of the laminar flame used to train the database. Figures 4–19 provide the PDFs and the scatter plots of Y_H and Y_{OH} as a function of Y_{CO_2}.

It is possible to observe that case 5 displays oscillations in the PDF, especially for Y_H (Fig. 12). This is due to the flame discretization on the mesh. Indeed the case is laminar (see Fig. 1) and initialized by extending the 1-D flame on the y-axis, leading to an oversampling of specific species values. Since the flame is propagating along the x-axis in a laminar manner, such over-representation results in higher probability for the repeated values, thus explaining the observed peaks in the PDF. Although less obvious, this can be observed on case 1 as well. This is confirmed by the scatter plots in Figs. 5 and 13.

Comparing the Y_H scatter plots as well as the conditioned PDFs for the different investigated cases, it is possible to conclude that turbulence strongly affects the original manifold. While case 1 and 5 display PDFs close to the original training data (Figs. 4 and 12), case 3 on Fig. 8 differs completely. Regarding the performances of the reduced models, it is clear that the score-PCA method (using the VARIMAX rotation) is able to follow more closely the DNS results, while the MG-PCA appears constrained to the laminar conditioned PDF. When the flame regime is the flamelet one, as for case

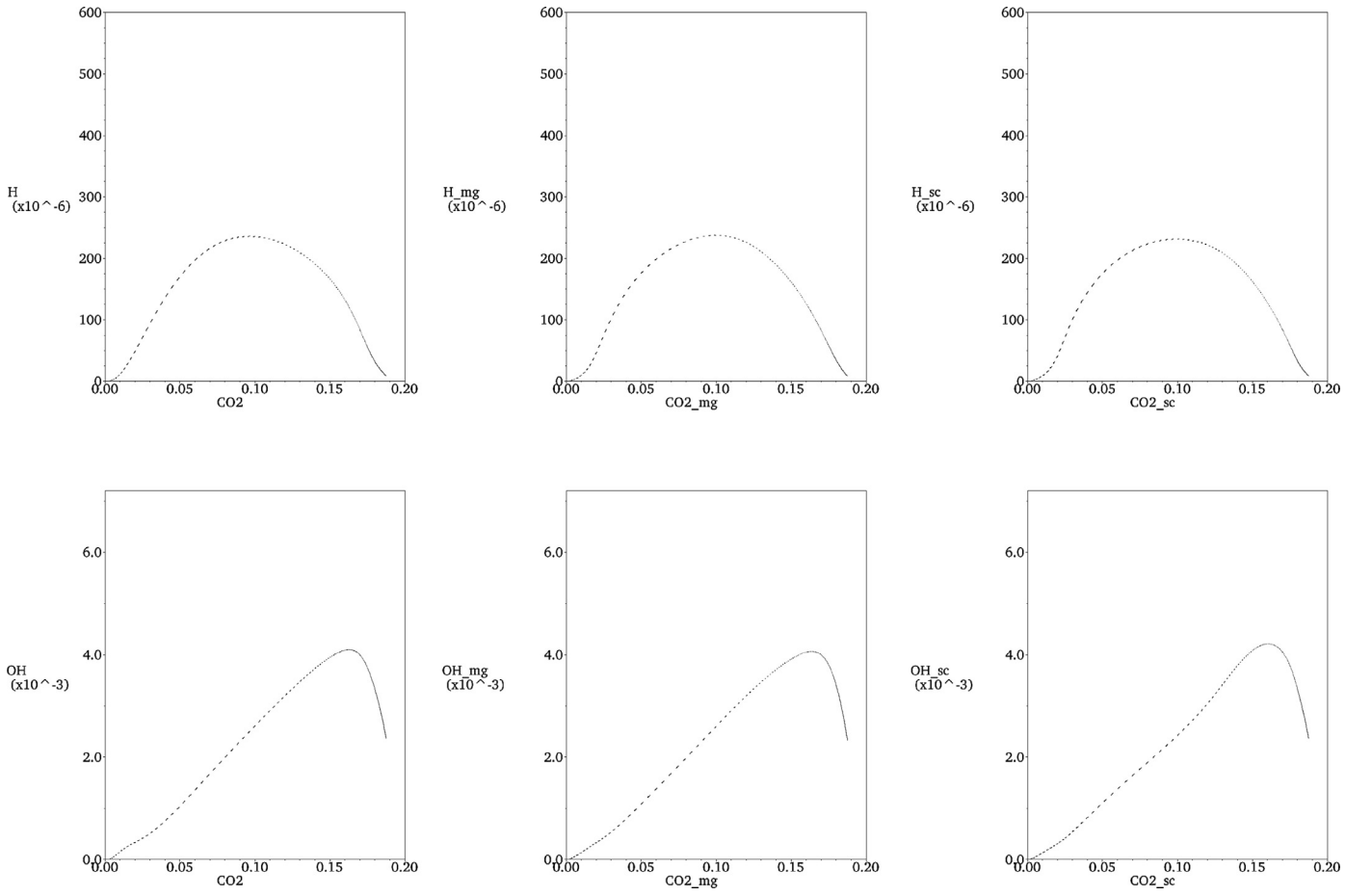

Fig. 13. Scatter plots of Y_H vs Y_{CO_2} for case 5, using DNS (left), MG-PCA (center) and score-PCA (right).

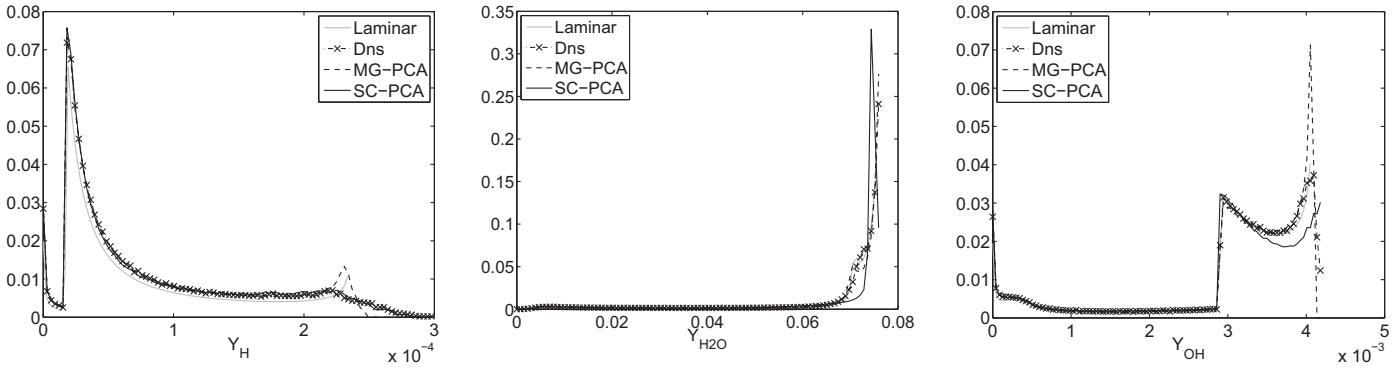

Fig. 14. Conditional PDF of Y_H, Y_{H_2O} and Y_{OH} for case 6.

1 and 5, MG-PCA is able to provide very accurate results. However, for cases where turbulence plays a major role on the flame structure, MG-PCA is not able to correctly capture the deviation from the original manifold, especially for high value of Y_H.

When considering the scatter plots for Y_H (Figs. 5,7,9,11,13,15,17 and 19), similar observations can be drawn. Score-PCA well mimics the distributions obtained with DNS for all cases, except for case 3 (Fig. 9), while MG-PCA results in a flame structure which is very close to the laminar one, as indicated by the small amount of scatter in Y_H distribution. Concerning case 3, it is interesting to point out that DNS displays a *two-branches* configuration, one around the laminar manifold and one above (Fig. 9). While MG-PCA captures only a small deviation from the training dataset, score-PCA is able to predict the *two branches* behavior, although without the desired accuracy.

The above observations can be directly extended to the analysis of Y_{OH} distribution. Score-PCA predicts correctly the deviation from the training dataset, while MG-PCA tends to overlap with it. Indeed when considering a well stirred reactor case like case 2, Fig. 6 indicates that MG-PCA provides a PDF close to the laminar flame one, while score-PCA follows more closely the DNS statistics (Fig. 8). MG-PCA can provide results superior to score-PCA only when operating very close to the flamelet regime, as it happens for cases 1, 5 and 8 (Figs. 4,5,12,13,18,19).

As far as case 3 is concerned (Figs. 8 and 9), the two branches are also observed for Y_{OH}. While the scatters plots (Fig. 9) indicates

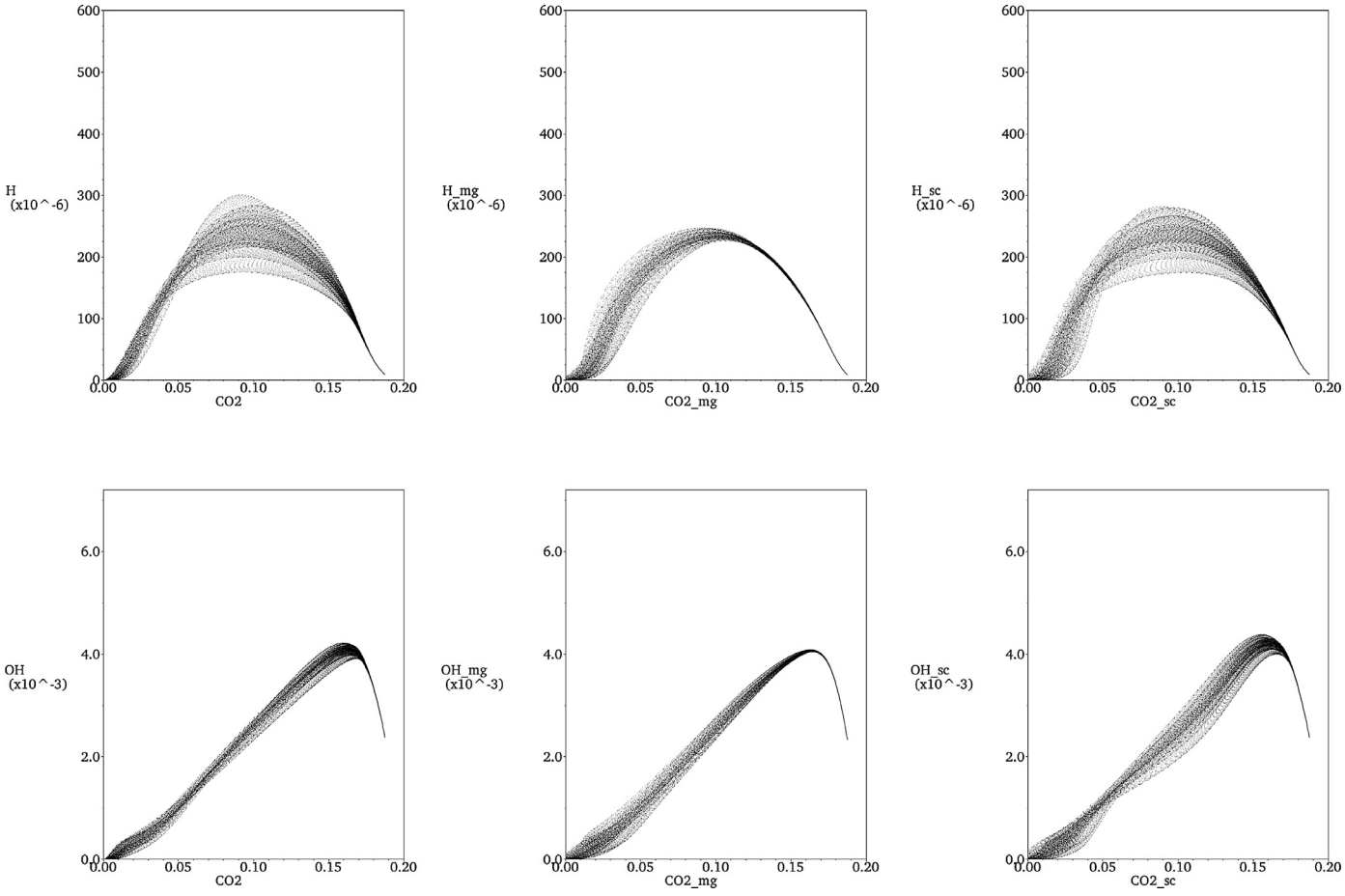

Fig. 15. Scatter plots of Y_H vs Y_{CO_2} for case 6, using DNS (left), MG-PCA (center) and score-PCA (right).

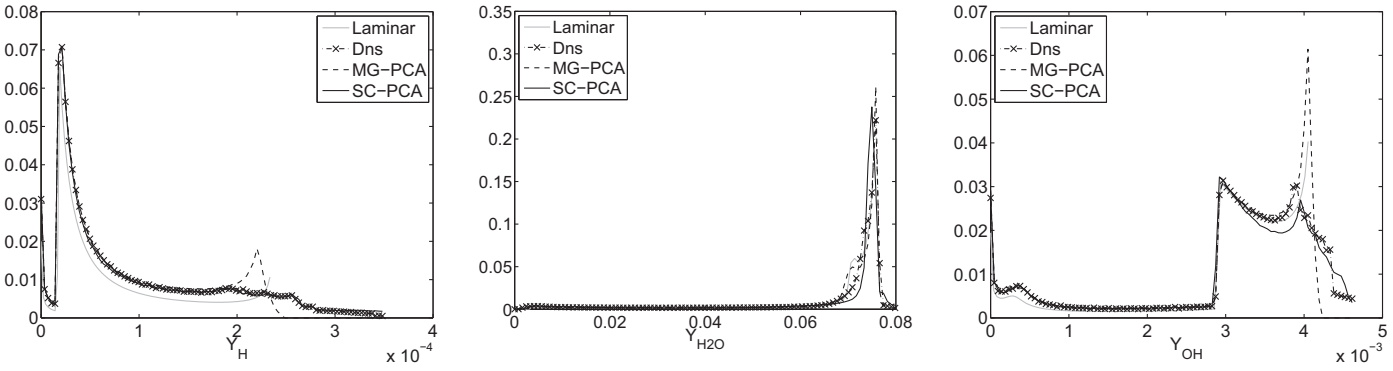

Fig. 16. Conditional PDF of Y_H, Y_{H_2O} and Y_{OH} for case 7.

a significant difference between score-PCA and DNS, the analysis of the PDFs suggest that the statistics provided by the two simulations do not differ strongly. The analysis of Y_H and Y_{OH} distribution indicate that score-PCA is able to capture the two branches behavior of case 3, using the information contained in the 1-D flame only. However, since the combustion regime for case 3 is significantly different than a laminar flame, the score-PCA predictions are not accurate.

From the analysis of Y_{H_2O} distribution, it appears that both methods behave well. However, MG-PCA is able to capture the first peak around 0.07, providing better results for cases 1, 5, 6 and 8 (see Figs. 4,12,14,18 respectively), which are all close to the flamelet regime in the Borghi diagram (Fig. 1). This confirms, as indicated previously, that MG-PCA results in better predictions for cases close to the original training dataset. On the other hand, for regimes far from the original one, score-PCA is able to better capture the deviation from the original manifold, while MG-PCA appears constrained to it. This is especially obvious for case 3 and 7, which are quite far from the laminar flame used to train the model (see Figs. 8 and 16, respectively).

In conclusion, both reduced models can provide very accurate results when the departure from the flamelet regime is not severe, representing an attractive alternative to tabulation techniques as FPI [25] or SLFM [26]. Far from the flamelet regime, the score-PCA approach is able to correctly reproduce the departure of the system from the original manifold, while MG-PCA appears to be constrained to that manifold. Interestingly, none of the methods produce numerical instabilities, which could

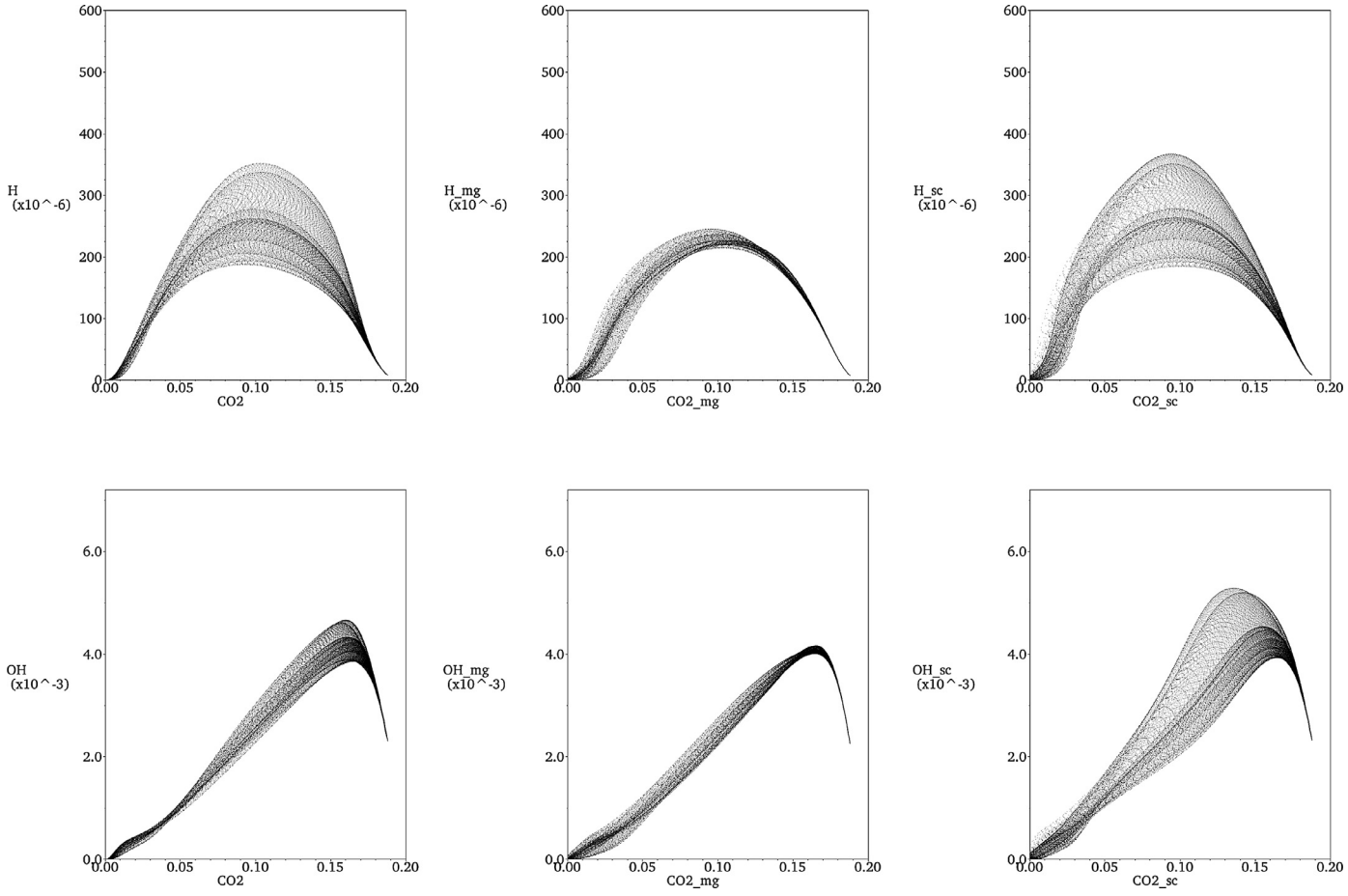

Fig. 17. Scatter plots of Y_H vs Y_{CO_2} for case 7, using DNS (left), MG-PCA (center) and score-PCA (right).

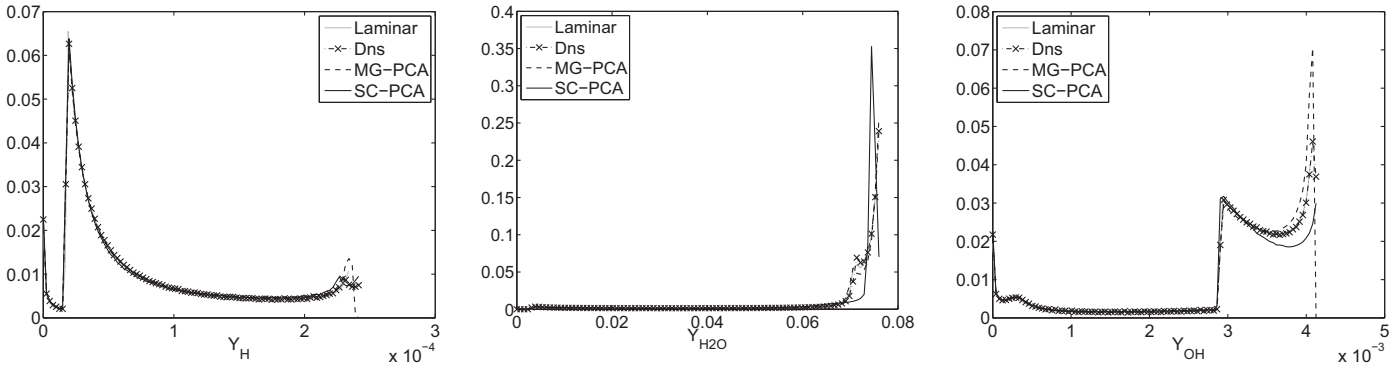

Fig. 18. Conditional PDF of Y_H, Y_{H_2O} and Y_{OH} for case 8.

yield to the simulation failure. Let's recall here that no artificial stabilization (like a tabulation of the source terms [11,17]) is used here, emphasizing the numerical stability of the methods. Finally, in terms of CPU time, both score-PCA and MG-PCA result in a speed-up of $\approx$ 31% with respect to DNS.

6. Conclusions

This study presented an in-depth analysis of method for the parametrization of the thermo-chemical state using two formulations of PCA-based models variations of PCA: score-PCA and MG-PCA. This study demonstrated that both methods accurately treat cases in which differential diffusion is not taken into account. When differential diffusion is considered, the score-PCA requires a rotation in order to diagonalize its diffusion matrix. Here the VARIMAX rotation was chosen to preserve the variance (i.e. the information) transported by the scores.

Section 5.2 proved that the score-PCA approach is able to better predict the deviation from the training dataset when flame-turbulence interactions are considered. On the other hand, MG-PCA performs well only when the investigated configurations do not significantly differ from the one characterizing the training dataset, i.e. flamelet regime. From a modeling point of view the score-PCA method is then superior to MG-PCA. Furthermore, score-PCA does not require any selection of transported species, which is a crucial step for the quality of MG-PCA results (see Isaac et al. [17]).

MG-PCA offers two advantages over the score-PCA approach. It requires minor code modifications and it can be very easily

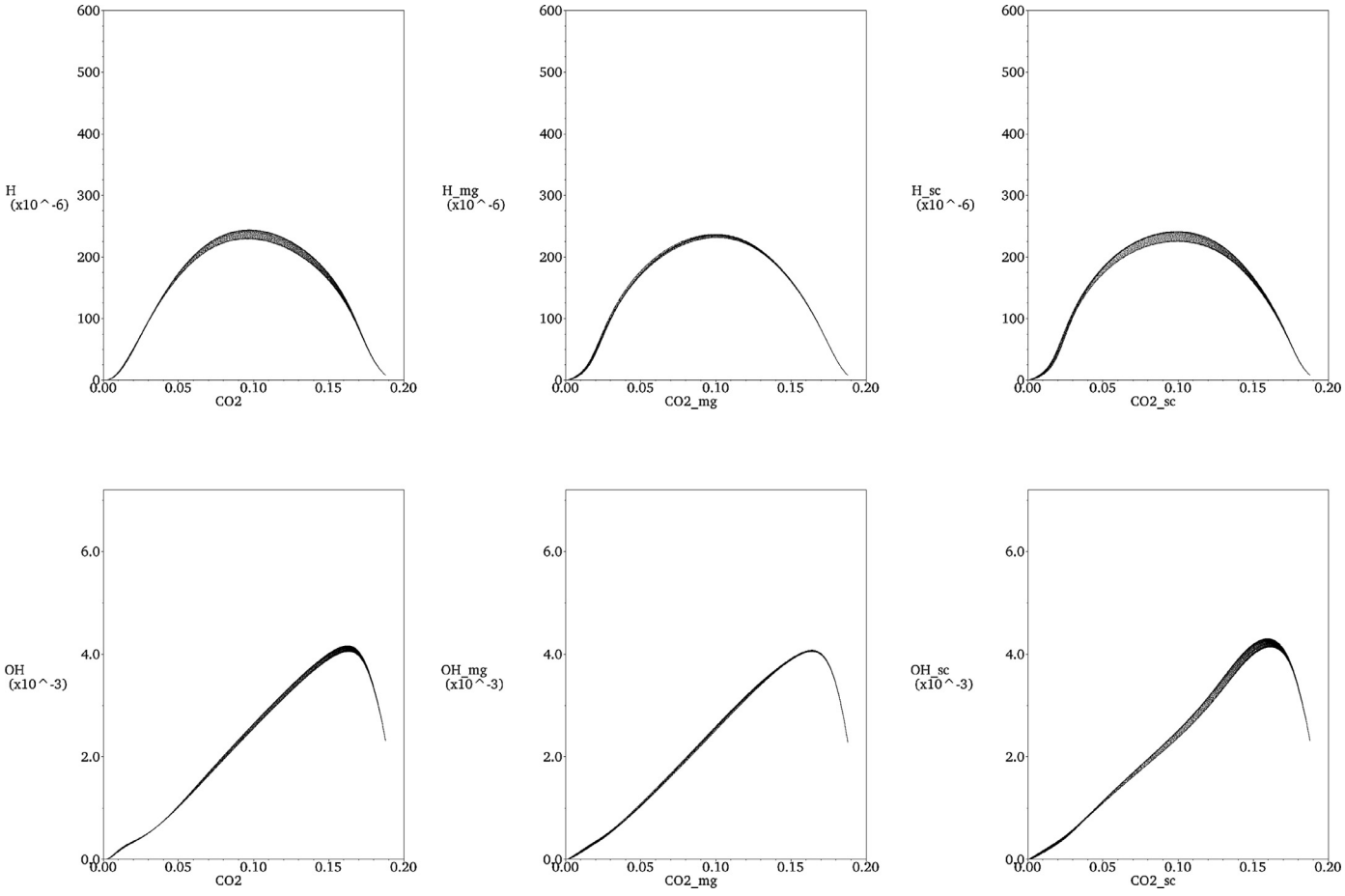

Fig. 19. Scatter plots of Y_H vs Y_{CO_2} for case 8, using DNS (left), MG-PCA (center) and score-PCA (right).

formulated for clusters [9], thus reducing the number of transported species. The local formulation appears challenging for the score approach, since the base change between clusters leads to a modification of PCs transport equations, thus multiplying the problem dimensions.

Finally, for both methods, a combination of both fast and slow chemical species is used in the set of transported variables, thus indicating that the reduced model do not guarantee a reduction of the problem stiffness. In the context of score-PCA a stiffness reduction is observed only when a small number of PCs is considered, in combination with non-linear regression methods.

Acknowledgments

The first author was supported by a fellowship from the Fonds National de la Recherche Scientifique, FRS-FNRS (Communauté Française de Belgique). This material is based on work supported by the Department of Energy, National Nuclear Security Administration, under Award Number(s) DE-NA0002375. The last author would like to acknowledge the support of Fédération Wallonie-Bruxelles, via Les Actions de Recherche Concerte (ARC) call for 2014-2019, to support fundamental research.

References

[1] J. Chen, A. Choudhary, B. de Supinski, M. DeVries, E. Hawkes, S. Klasky, W. Liao, K. Ma, J. Mellor-Crummey, N. Podhorszki, et al., Terascale direct numerical simulations of turbulent combustion using s3d, Comput. Sci. Discov. 2 (2009) 015001.
[2] K. Pearson, On lines and planes of closest fit to systems of points in space, Philos. Mag. Ser. 6 2 (11) (1901) 559–572.
[3] I. Jolliffe, Principal component analysis, Wiley Online Library, 2002.
[4] J.E. Jackson, A user's guide to principal components, vol. 587, John Wiley & Sons, 2005.
[5] J. Sutherland, A. Parente, Combustion modeling using principal component analysis, Proc. Combust. Inst. 32 (1) (2009) 1563–1570.
[6] A. Parente, J.C. Sutherland, Principal component analysis of turbulent combustion data: Data pre-processing and manifold sensitivity, Combust. Flame 160 (2) (2013) 340–350.
[7] A. Coussement, O. Gicquel, A. Parente, Kernel density weighted principal component analysis of combustion processes, Combust. Flame 159 (9) (2012) 2844–2855.
[8] A. Biglari, J.C. Sutherland, A filter-independent model identification technique for turbulent combustion modeling, Combust. Flame 159 (5) (2012) 1960–1970.
[9] A. Coussement, O. Gicquel, A. Parente, MG-local-PCA method for reduced order combustion modeling, Proc. Combust. Inst. 34 (1) (2013) 1117–1123.
[10] H. Mirgolbabaei, T. Echekki, A novel principal component analysis-based acceleration scheme for LES-ODT: An a priori study, Combust. Flame 160 (5) (2013) 898–908.
[11] T. Echekki, H. Mirgolbabaei, Principal component transport in turbulent combustion: A posteriori analysis, Combust. Flame 162 (5) (2015) 1919–1933.
[12] B.J. Isaac, J.N. Thornock, J.C. Sutherland, P.J. Smith, A. Parente, Advanced regression methods for combustion modelling using principal components, Combust. Flame 162 (6) (2015) 2592–2601.
[13] A. Parente, J. Sutherland, L. Tognotti, P. Smith, Identification of low-dimensional manifolds in turbulent flames, Proc. Combust. Inst. 32 (1) (2009) 1579–1586.
[14] S.B. Pope, Small scales, many species and the manifold challenges of turbulent combustion, Proc. Combust. Inst. 34 (1) (2013) 1–31.
[15] Y. Yang, S.B. Pope, J.H. Chen, Empirical low-dimensional manifolds in composition space, Combust. Flame 160 (10) (2013) 1967–1980.
[16] H. Mirgolbabaei, T. Echekki, Nonlinear reduction of combustion composition space with kernel principal component analysis, Combust. Flame 161 (1) (2014) 118–126.
[17] B.J. Isaac, A. Coussement, O. Gicquel, P.J. Smith, A. Parente, Reduced-order PCA models for chemical reacting flows, Combust. Flame 161 (11) (2014) 2785–2800.
[18] A. Coussement, O. Gicquel, J. Caudal, B. Fiorina, G. Degrez, Three-dimensional boundary conditions for numerical simulations of reactive compressible flows with complex thermochemistry, J. Comput. Phys. 231 (17) (2012) 5571–5611.

[19] A. Coussement, O. Gicquel, B. Fiorina, G. Degrez, N. Darabiha, Multicomponent real gas 3-d-nscbc for direct numerical simulation of reactive compressible viscous flows, J. Comput. Phys. 245 (2013) 259–280.
[20] M. Ó Conaire, H. Curran, J. Simmie, W. Pitz, C. Westbrook, A comprehensive modeling study of hydrogen oxidation, Int. J. Chem. Kinet. 36 (11) (2004) 603–622.
[21] S.G. Davis, A.V. Joshi, H. Wang, F. Egolfopoulos, An optimized kinetic model of H2/CO combustion, Proc. Combust. Inst. 30 (1) (2005) 1283–1292.
[22] R. Kee, F. Rupley, E. Meeks, J. Miller, CHEMKIN-III: A FORTRAN chemical kinetics package for the analysis of gas-phase chemical and plasma kinetics, Report SAND96-8216, Sandia National Laboratories, 1996.
[23] H.F. Kaiser, The varimax criterion for analytic rotation in factor analysis, Psychometrika 23 (3) (1958) 33–3123.
[24] T. Passot, A. Pouquet, Numerical simulation of compressible homogeneous flows in the turbulent regime, J. Fluid Mech. 181 (1987) 441–466.
[25] O. Gicquel, N. Darabiha, D. Thévenin, Laminar premixed hydrogen/air counterflow flame simulations using flame prolongation of ILDM with differential diffusion, Proc. Combust. Inst. 28 (2) (2000) 1901–1908.
[26] N. Peters, Laminar diffusion flamelet models in non-premixed turbulent combustion, Prog. Energy Combust. Sci. 10 (3) (1984) 319–339.